Nanoscale

Accepted Manuscript

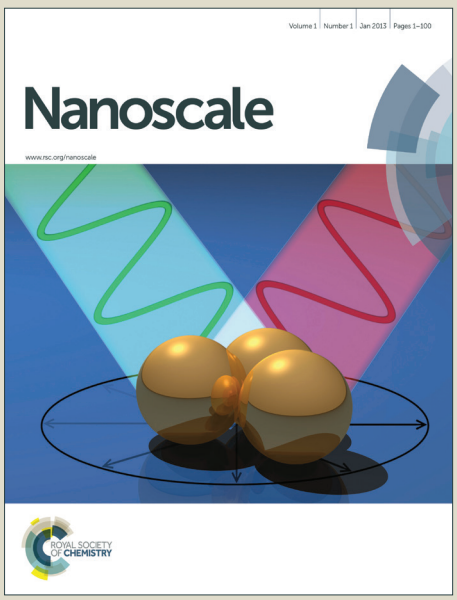

ROYAL SOCIETY OF CHEMISTRY

www.rsc.org/nanoscale

Cite this: DOI: 10.1039/c0xx00000x

www.rsc.org/xxxxxx

COMMUNICATION

Triple-layer nanostructured WO_3 photoanodes with enhanced photocurrent generation and superior stability for photoelectrochemical solar energy conversion

Huan Qi,[a] Jonathan Wolfe,[b] Danping Wang,[e] Hong Jin Fan,[c] Denis Fichou*[c,d] and Zhong Chen*[a,e]

Received (in XXX, XXX) Xth XXXXXXXXX 20XX, Accepted Xth XXXXXXXXX 20XX
DOI: 10.1039/b00000

Unique nanorods/nanoparticles/nanoflakes (NRs/NPs/NFs) WO_3 triple-layers are grown on a metallic W foil by a simple one-step anodization method. The triple-layer structure is formed through a self-organization process, the film thickness (up to 3 µm) being controlled by the anodization time. A first layer made of an array of WO_3 densely-packed vertically-aligned NRs (1.2-1.4 µm in height) grow atop the tungsten foil, followed by a second layer of small NPs (50-80 nm) and finally a third layer made of rectangular NFs (200-300 nm). When irradiated by white light in a photoelectrochemical cell these WO_3 triple-layers generate a photocurrent as high as 0.9 mA.cm^{-2} at 1.2 V/RHE. Moreover, we show that the stability of the triple-layer WO_3 photoanodes can be considerably enhanced by adding an ultrathin (10 nm) TiO_2 protective overlayer.

It has long been a dream for mankind to efficiently convert sunlight into clean and readily usable fuels such as hydrogen and methane on a large scale.[1] Over the past decades intensive research efforts have been devoted to this challenge and various materials and technologies have been explored in view of solar light conversion and storage.[2] One of the most promising technologies consists in splitting water into hydrogen and oxygen through solar irradiation of semiconductor-based devices. Ever since the first work on a TiO_2-based system,[3] metal oxide semiconductors have become a promising arsenal of materials for water splitting applications, particularly in photoelectrochemical (PEC) systems.[4] Though TiO_2 is the most commonly used material in PEC applications, its wide band-gap (3.0-3.2 eV) hinders its light harvesting efficiency within the visible range of the solar spectrum. Various approaches to extend TiO_2 absorption into the visible range have been investigated, prominently 3d-metal doping, dye sensitization and quantum dots. However these approaches reveal to be costly thus limiting their commercial applications.[5] Therefore, the quest for alternative visible-light photosensitive and earth-abundant semiconductors is focusing the attention of researchers worldwide.

Among the promising novel energy-related materials, tungsten trioxide WO_3 recently proved to be a very attractive photoanode material in PEC architectures for the following reasons. First, WO_3 possesses a band-gap of ≈2.6 eV,[6] thus allowing its utilization in part of the visible range of the solar spectrum. Then, the theoretical maximum conversion efficiency of WO_3 is ≈6.3% for photons having energies higher than 2.6 eV.[7] Moreover, WO_3 exhibits an important hole diffusion length (≈150 nm),[8] as compared to other semiconducting metal oxides. All these properties render WO_3 a suitable candidate as a photoanode material in PEC applications.

In view of maximizing the surface-to-volume ratio, a large variety of WO_3 nanostructures have been reported. These include nanoflakes,[9] nanoparticles,[10] nanorods,[8] nanowires,[11] nanoplatelets,[12] and some unconventional morphologies such as wormlike[13] and wedgelike[14] structures. The photoactivity of WO_3 is determined by its crystalline structure which can be either hexagonal, orthorhombic or monoclinic depending on the preparation method and post-annealing conditions. Among these three phases the monoclinic one is the most stable at room temperature. Both monoclinic and hexagonal phases display superior PEC water splitting capability in comparison with the orthorhombic hydrated phase.[15]

We report here on a new type of nanostructured WO_3 photoanode constituted of a nanorods/nanoparticles/nanoflakes (NRs/NPs/NFs) triple layer architecture. The triple-layer WO_3 films are fabricated by a simple time-controlled anodization method of tungsten foils with the assistance of fluorine and nitric acid co-etching effect at high temperature. After annealing, the WO_3 triple-layers are monoclinic. The PEC performances of several WO_3 photoanodes having either one, two or three layers obtained with different anodization times are systematically investigated, revealing the superior photocurrent generation of triple-layers over single- and double-layers. Finally we show that the stability of the triple-layer WO_3 in a neutral electrolyte can be considerably enhanced after deposition of a thin (10 nm) TiO_2 overcoating by means of atomic layer deposition.

The successive anodization steps of W foils leading to WO_3 nanostructured overlayers are illustrated in Figure 1. Within the first hour the starting tungsten foil is first anodized into a densely-packed array of vertically-oriented WO_3 nanorods (NRs) along an oxidation reaction. One of the advantages of this packed NRs layer is to preserve good structural continuity between tungsten and WO_3. Such a structural continuum will allow to efficiently transfer photocarriers from the oxide surface to the W substrate in PEC experiments. In a second step, the fluorine/nitric acid co-etching effect produces a porous nanoparticles (NPs) layer followed by a loose nanoflakes (NFs) layer.

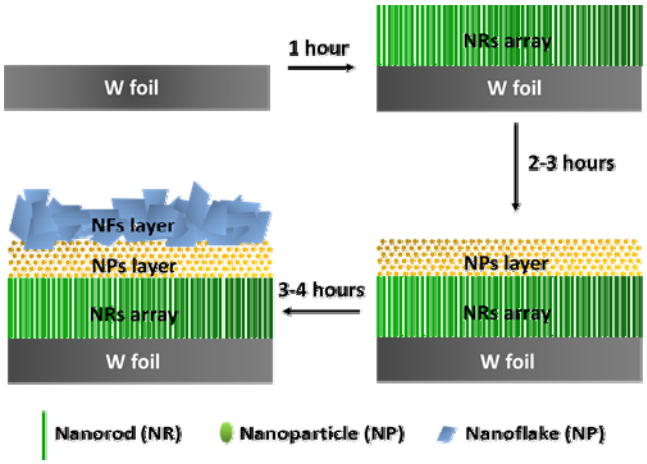

Fig. 1 Scheme of the three-step growth of a {NRs (1.4 µm)/NPs (1.0 µm)/NFs (0.5 µm)} WO_3 triple-layer by anodization of a W foil. The growth times of the nanorods (NRs), nanoparticles (NPs) and nanoflakes (NFs) layers are 1, 2-3 and 3-4 hours respectively.

Such a nanostructured triple-layer morphology provides an optimized surface area to harvest a maximum number of incident photons as well as more sites for hole injection.

Figure 2 shows the top and cross-sectional morphologies of the WO_3 layers as observed by FESEM. By fine-tuning the parameters of the W oxidation such as in particular the fluorine concentration, temperature and anodization voltage, the thickness and nanostructure of the NRs/NPs/NFs triple-layer structure can be adjusted. After one hour, an array of vertically-aligned WO_3 NRs grow on top of the W foil according to the chemical process below (see ESI, Fig. S1):[16]

$$W + 2H_2O \longrightarrow WO_2^{2+} + 4H^+ \quad (1)$$

$$2\,WO_2^{2+} + 2H_2O \longrightarrow W_2O_5 + 2H^+ \quad (2)$$

$$W_2O_5 + H_2O \longrightarrow 2\,WO_3 + 2H+ \quad (3)$$

These reactions occur under relatively high voltage (30 V) and in a fluorine-free electrolyte, which means NH_4F does not involve in this reaction for nanorod growth disregard its existence. The effect of fluorine starts from the growth of nanoparticle. In the first step of anodization, W is oxidized into $W^{4+/}W^{6+}$ due to the high voltage. Then W^{4+}/W^{6+} react with penetrated O^{2-} into WO_2^{2+} close to the surface of the W foil (eq. 1). Subsequently, WO_2^{2+} is oxidized into W_2O_5 (eq. 2) which further oxidizes into the more stable WO_3 NRs array (eq. 3).

Because oxidization is a self-limiting process due to the poor penetration of oxygen atoms inside the W foil, the addition of fluorine ions can increase the thickness of metal oxide and act as a capping agent for crystal growth.[17] Meanwhile, the F^- anions dissolve the metal oxide to form fluorine complexes according to equation 4-5.[18] A porous NPs layer resulting from the following reaction is also spotted on top of the NRs array (Fig. 2b).

$$W^{4+} + 6F^- \longrightarrow WF_6^{2-} \quad (4)$$

$$W^{6+} + 8F^- \longrightarrow WF_8^{2-} \quad (5)$$

The outermost layer of the WO_3 thin film is composed of nanoflakes NFs. These flakes arise from the etching effect of the HNO_3/NH_4F acidic electrolyte at high temperature.[19] Acid etching is a reaction based on Pourbaix diagram (potential *vs* pH) in pH=1 environment, first forming WO_4^{2-} species that convert into WO_3.[19]

During such a chemical process both temperature and pH play important roles in the final WO_3 NFs morphology, according to eq. 6.

$$WO_4^{2-} + 2H^+ \longrightarrow WO_3 + H_2O \quad (6)$$

However, acid etching is usually a very slow process with etching speed in the range 0.5-1.0 µm.h^{-1} at 50°C (which is the temperature used here), and the flake size is quite large (diameter >500 nm).[20] In comparison, in our process the F^- anions induce a faster etching that results in flakes of substantially smaller size (diameter≈200-300 nm). Co-etching by both HNO_3 and NH_4F leads to the NPs/NFs bilayer nanostructure whose high roughness, inducing high surface area, is favorable to an efficient photon absorption (see ESI, Fig. S2). Compared with similar NRs/NFs double layered WO_3 reported earlier using nitric acid,[21] the microstructure in the current work is finer and more uniform due to the above explained role of F^- ions.

Another advantage provided by the unique NRs/NPs/NFs triple layers is that the density gradually evolves from densely-packed

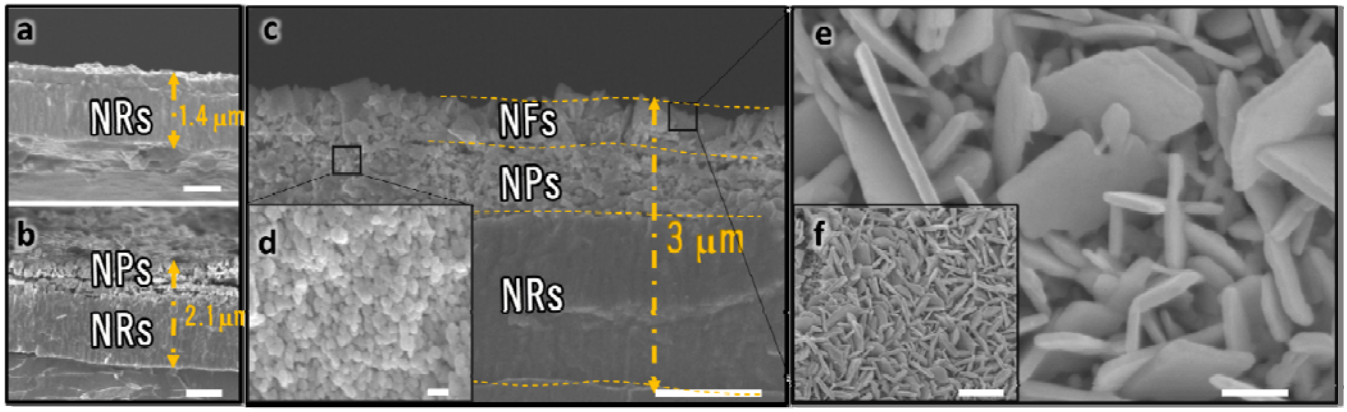

Fig. 2 FESEM cross-sectional micrographs of WO_3 layers after anodization of a W foil during (a) 1 hour: NRs layer, (b) 2-3 hours: NRs/NPs bilayer, and (c) 3-4 hours: NRs/NPs/NFs triple layer. (d) FESEM cross-sectional view of nanoparticles NPs and (e, f) FESEM top view of nanoflakes NFs after anodization for 4 hours (f) The scale bars represent 1 µm for a-c,f and 100 nm for d,e.

Cite this: DOI: 10.1039/c0xx00000x

www.rsc.org/xxxxxx

COMMUNICATION

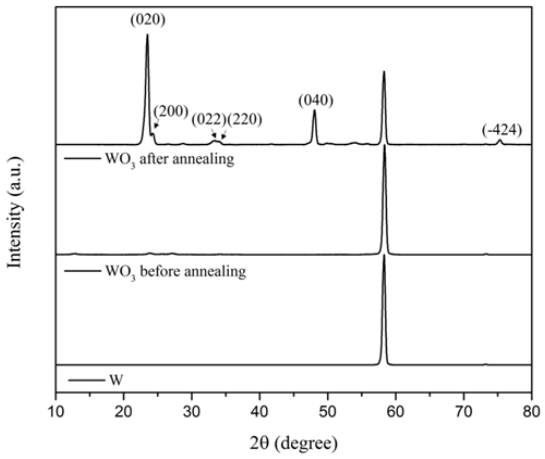

Fig. 3 XRD spectra of (a) a tungsten foil before anodizing, (b) as-anodized WO_3, and (c) WO_3 after annealing at 550 °C for 4 hours.

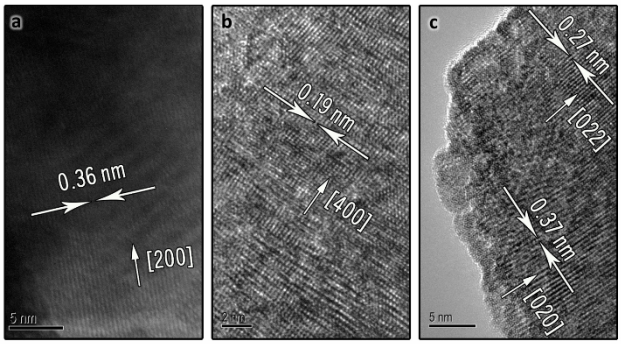

Fig. 4 HRTEM images of (a) an individual WO_3 nanorod, (b) a nanoparticle and (c) a nanoflake. The crystallographic growth directions and lattice spacings are indicated. The scale bar represents 5 nanometers (a and c) or 2 nanometers (b).

NRs to porous NPs and to disconnected NFs. Such a surface morphology results in a reduced reflectance and an increased photon absorption and charge carrier generation.

The photon absorption of the WO_3 triple layers was evaluated through the reflectance spectra (see ESI, Fig. S3). The spectra show that the samples prepared under anodization times in the range 1-3 hours exhibit similar absorption features. However, after 4 hours of anodization the samples exhibit a lower reflectance, hence a higher absorbance, induced by the unique NFs structure. These loose NFs layers ensure an optimized photon absorption because of an important area, which then give rise to photocarriers, while the NPs and NRs layers ensure transport of photogenerated electrons toward the metallic W foil.

The XRD patterns of an anodized W foil before and after annealing are shown in Figure 3. Before annealing (Fig.3b) the diffraction pattern is essentially similar to that of tungsten,

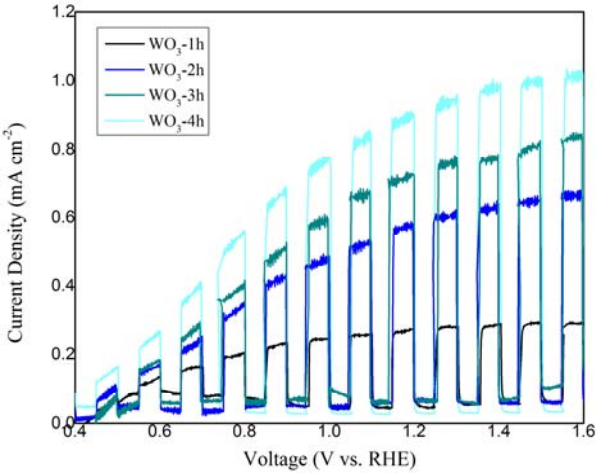

Fig. 5 Linear sweep voltamperograms of WO_3 photoanodes under incident chopped light (f=0.2 Hz) for anodization times of respectively 1, 2, 3 and 4 hours.

showing the amorphous character of WO_3 at this stage. In sharp contrast, after annealing at 550°C for 4 hours (Fig.3c), amorphous WO_3 turned into a crystalline monoclinic phase, as revealed by the appearance of two intense XRD peaks at 24.3° and 75.3°, attributed to the (200) and (040) planes respectively.

Figure 4 shows typical HRTEM images of individual monoclinic WO_3 nanoflake, nanoparticle and nanorod. High-resolution reveals that NRs grow along the [200] crystallographic direction. In turn, NPs grow along the [400]. Finally NFs grow along both [022] and [020] with lattice spacings of 0.27 and 0.37 nm respectively. Meanwhile, TEM images reveal the diameter of NRs is ≈50nm (see ESI, Fig. S4). The HRTEM results correspond with the XRD data, and further prove the good crystallinity property (monoclinic) of as prepared WO3 thin film.[15]

The PEC properties of as-prepared triple-layer WO_3 thin films were evaluated using pulsed linear sweep voltammetry (LSV). Figure 5 shows that the highest photocurrent density (0.9 $mA.cm^{-2}$ at 1.2 V vs RHE) is observed after a 4 hour anodization time. For shorter anodization periods (1-3 hours) the photocurrents are considerably lower, thus revealing the importance of having a triple layer structure. The LSV comparison between triple-layer WO_3 and single-layer WO_3 with similar thickness further proved the superior PEC properties of as prepared triple-layer WO_3 (see ESI, Fig. S5). Furthermore, incident photon-to-current efficiency (IPCE) graph shows 42% conversion efficiency under 420 nm illumination (see ESI, Fig. S6).

The superior performances of WO_3 anodized during 4 hours arises from a more efficient charge separation and a faster interfacial charge transfer,[22] as revealed by electrochemical impedance spectroscopy (EIS, Fig. 6a). The EIS plots in Figure 6b show that the difference in Nyquist arc of as-prepared WO_3 in

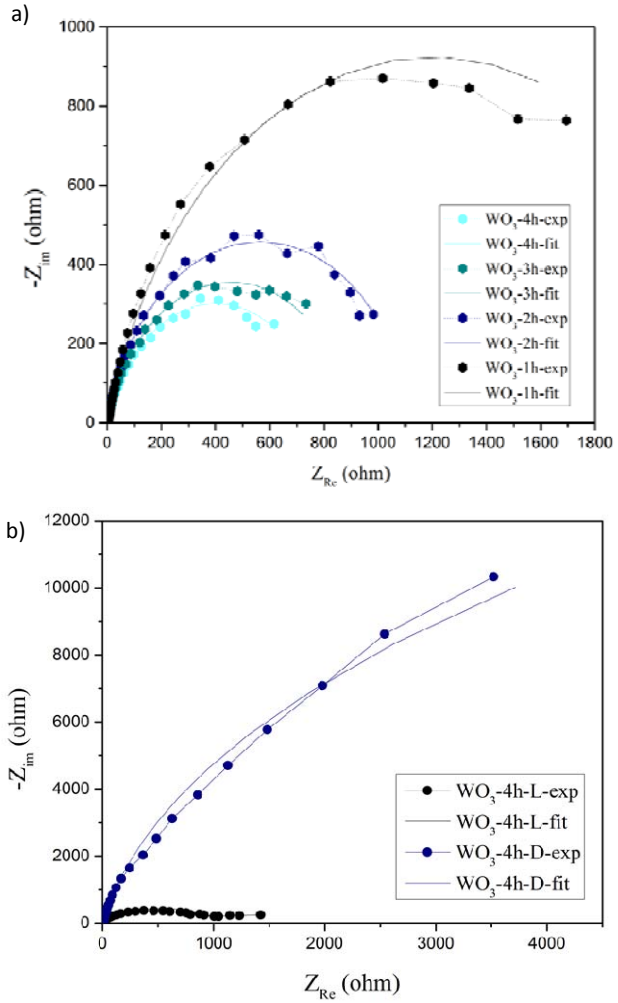

Fig. 6 Nyquist experimental data and fitting plots after anodization during (a) 1h, 2h ,3h and 4h under illumination and (b) 4h either in the dark (blue dots) or under illumination (black dots).

dark and illumination conditions, which shows the light-generated electron improves the conductivity of WO_3 photoanode.

Equivalent circuit modelling is based on the impedance experimental data, which is plotted as real admittance *vs.* imaginary admittance. The data configuration in Figure 6 is within the first quadrant, thus implying that no inductance is needed.[23]

Our model is shown in Figure 7a, whereas other models have also been used in PEC cell studies.[24] It consists in two resistances R_1 and R_2 and one constant phase element (CPE) working as a non-ideal capacitor. R_1 represents the material resistive loss predominantly at the interface of the material surface and the electrolyte, and R_2 represents the internal electron-hole recombination resistance including the recombination happening within the depletion layer. The R_1 and R_2 values derived from the impedance data are summarized in Figure 7b.It can be observed that the samples anodized during 4 hours possess both the smallest interface and internal resistances, thus explaining the origin of its higher PEC capability.

However, although the WO_3 triple layers exhibit excellent PEC

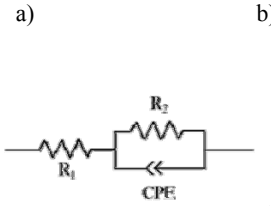

b)

Sample	R_1 (ohms)	R_2 (ohms)
WO_3-1h	3.484	2398
WO_3-2h	2.069	1126
WO_3-3h	2.049	910.1
WO_3-4h	1.833	799.2

Fig. 7 (a) Proposed equivalent circuit consisting in a constant phase element (CPE) working as a non-ideal capacitor, an interface resistance R_1 and an internal electron-hole recombination resistance R_2. (b) Resistance values R_1 and R_2 as obtained from the EIS measurements.

properties, they suffer from chemical dissolution in pH value greater than 5 solutions, thus affecting the photocurrent.[25] In order to prevent this drawback, a 10 nm-thin TiO_2 layer is coated on top of the WO_3 NRs/NPs/NFs triple-layer.

Comparative PEC stability tests on WO_3 triple layers with and without a TiO_2 protective layer are conducted in pH=7 buffer solutions under a constant bias of 0.8 V *vs* RHE (Fig. 8). During PEC tests, the samples are illuminated during 50 seconds with periods in the dark of varying duration in the range 0.5-4.0 hours.

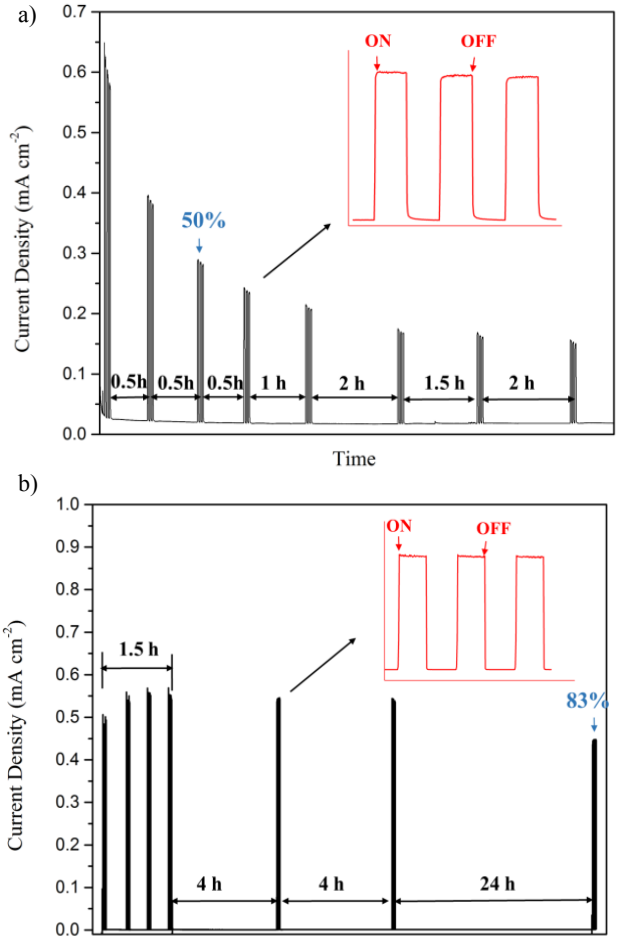

Fig. 8 PEC stability tests of (a) an as-grown WO_3 triple-layer, and (b) a WO_3 triple-layer coated by a 10 nm-TiO_2 overlayer. Tests are conducted in a pH=7 buffer solution under constant voltage 0.8V *vs* RHE. The inset is the chronoamperometry scan with periodic on/off light cycles. Incident light intensity: 100 mW.cm^{-2}; illuminated sample area: 0.76 cm^2.

Figure 8 shows that unprotected WO_3 loses 50% of its original photocurrent within the first hour. In sharp contrast, there is no significant photocurrent loss detected for the TiO_2-protected WO_3 samples within the first 10 hours. Furthermore, when the PEC test is realized after an additional 24 hours, the recorded photocurrent remains as high as 83% of the initial one. This clearly demonstrates that the PEC photocurrent is three times higher with nanostructured NRs/NPs/NFs WO_3 triple layers as compared to single WO_3 layers and can also be stabilized under illumination by an ultrathin TiO_2 protective overlayer.

In summary, we describe here a new and simple strategy to fabricate well-defined nanostructured WO_3 NRs/NPs/NFs triple-layers acting as efficient photoanodes in PEC systems. The preparation of these WO_3 triple-layers consists in the anodization of a starting metallic W foil under control of time. For short anodization times (1 hour) the surface of the W foils oxidizes into a highly-ordered array of vertically-oriented WO_3 nanorods. For longer times (2-3 hours) a second layer made of nanoparticles grow atop the nanorods. Finally for anodization time of 4 hours a third layer made of nanoflakes appears, while longer times do not induce any further modification. After annealing, the WO_3 triple-layer exhibits a photocurrent of 0.90 mA cm^{-2} under 1.2 V bias vs RHE, that is three times higher than that obtained with a single-layer made of nanorods (0.32 mA cm^{-2}). With a 10 nm-thin TiO_2 protective coating, the WO_3 triple layer photoanodes exhibit a superior stability without any significant loss in photocurrent over 10 hours of continuous illumination. As a perspective, further improvement in PEC stability can probably be achieved by increasing slightly the thickness of the TiO_2 protective layer. With such optimized morphological and PEC properties, as well as suitable band positions (see ESI, Fig. S7-8), we believe that these novel nanostructured WO_3 NRs/NPs/NFs triple-layers can be very useful in other PEC systems, especially in view of artificial photosynthesis.

Acknowledgements

One of us (DF) wishes to thank the Division of Physics and Applied Physics (PAP), School of Physical and Mathematical Sciences (SPMS) at Nanyang Technological University (NTU), Singapore, for a position of Visiting Professor. The support from Singapore National Research Foundation (NRF) through the Singapore-Berkeley Research Initiative for Sustainable Energy (SinBeRISE) CREATE Programme is highly appreciated.

Notes and references

[a] *School of Materials Science Engineering, Nanyang Technological University, Singapore 639798, Singapore. Tel: +65 67904256; E-mail: aszchen@ntu.edu.sg*

[b] *Interdisciplinary Graduate School, Nanyang Technological University, Singapore 639798, Singapore.*

[c] *School of Physical and Mathematical Sciences, Nanyang Technological University, 637371, Singapore.*

[d] *Sorbonne Universités, UPMC Univ Paris 06, UMR 8232, Institut Parisien de Chimie Moléculaire, F-75005, Paris, France. Tel: +33 144275080; E-mail: denis.fichou@upmc.fr;*

[e] *Energy Research Institute at NTU (ERI@N), 1 CleanTech Loop, #06-04, CleanTech One, Singapore 6371412*

† Electronic Supplementary Information (ESI) available: [details of any supplementary information available should be included here]. See DOI: 10.1039/b000000x/

1. (a) K. Maeda, K. Teramura, D. L. Lu, T. Takata, N. Saito, Y. Inoue and K. Domen, *Nature*, 2006, **440**, 295; (b) J. A. Turner, *Science*, 2004, **305**, 972. (c) Z. Li, W. Luo, M. Zhang, F. Feng and Z. Zou, *Energy Environ. Sci.*, 2013, **6**, 347. (d) E. Alberico, P. Sponholz, C. Cordes, M. Nielsen, H. J. Drexler, W. Baumann, H. Junge and M. Beller, *Angew. Chem. Int. Ed*. 2013, **52**, 14162. (e) X. Ge, L. Chen, L. Zhang, Y. Wen, A. Hirata and M. Chen, *Adv. Mater.*, 2014, **26**, 3100.
2. (a) O. Khaselev and J. A. Turner, *Science*, 1998, **280**, 425; (b) Y. J. Lin, C. Battaglia, M. Boccard, M. Hettick, Z. B. Yu, C. Ballif, J. W. Ager and A. Javey, *Nano Lett.*, 2013, **13**, 5615; (c) I. S. Cho, Z. B. Chen, A. J. Forman, D. R. Kim, P. M. Rao, T. F. Jaramillo and X. L. Zheng, *Nano Lett.*, 2011, **11**, 4978. (d) X. Xia, Y. Zhang, D. Chao, C. Guan, Y. Zhang, L. Li, X. Ge, I. M. Bacho, J. Tu and H. J. Fan, *Nanoscale*, 2014, **6**, 5008.
3. A. Fujishima and K. Honda, *Nature* 1972, **238**, 37.
4. (a) J. B. Xue, Q. Q. Shen, W. Liang, X. G. Liu and F. Yang, *Electrochim. Acta*, 2013, **97**, 10; (b) C. T. Wang, H. L. Siao and Y. C. Chiu, *Surf. Coat. Tech.*, 2013, **232**, 658; (c) D. Fichou, J. Pouliquen, J. Kossanyi, M. Jakani, G. Campet and J. Claverie, *J. Electroanal. Chem.*, 1985, **188**, 167; (d) D. Fichou and J. Kossanyi. *J. Electrochem. Soc.*, 1986, **133**, 1607; (e) M. Jakani, D. Fichou, G. Campet, J. Claverie, J. Pouliquen and J. Kossanyi, *J. Solid State Chem*., 1985, **56**, 269.
5. (a) Z. W. Seh, S. H. Liu, M. Low, S. Y. Zhang, Z. L. Liu, A. Mlayah and M. Y. Han, *Adv. Mater*., 2012, **24**, 2310; (b) F. Zuo, K. Bozhilov, R. J. Dillon, L. Wang, P. Smith, X. Zhao, C. Bardeen and P. Y. Feng, *Angew. Chem. Int. Edit.*, 2012, **51**, 6223.
6. D. Chen, and J. H. Ye, *Adv Funct Mater*, 2008, **18**, 1922.
7. T. Bak, J. Nowotny, M. Rekas, C. C. Sorrell, *Int. J. Hydrogen Energ.*, 2002, **27**, 991.
8. S. S. Kalanur, Y. J. Hwang, S. Y. Chae and O. S. Joo, *J. Mater. Chem. A*, 2013, **1**, 3479.
9. (a) G. M. Wang, Y. C. Ling, H. Y. Wang, X. Y. Yang, C. C. Wang, J. Z. Zhang and Y. Li, *Energ. Environ. Sci.*, 2012, **5**, 6180-6187. (b) D. D. Qin, C. L. Tao, S. A. Friesen, T. H. Wang, O. K. Varghese, N. Z. Bao, Z. Y. Yang, T. E. Mallouk and C. A. Grimes, *Chem. Commun.* , 2012, **48**, 729. (c) Q. P. Chen, J. H. Li, B. X. Zhou, M. C. Long, H. C. Chen, Y. B. Liu, W. M. Cai and W. F. Shangguan, *Electrochem. Commun.*, 2012, **20**, 153. (d) J. R. Huang, X. J. Xu, C. P. Gu, G. J. Fu, W. Z. Wang and J. H. Liu, *Mater. Res. Bull.*, 2012, **11**, 3224.
10. H. Y. Wu, M. Xu, P. M. Da, W. J. Li, D. S. Jia and G. F. Zheng, *Phys. Chem. Chem. Phys.*, 2013, **15**, 16138.
11. Z. W. Liu, Y. Bando and C. C. Tang, *Chem. Phys. Lett.*, 2003, **372**, 179-182.
12. A. Z. Sadek, H. D. Zheng, M. Breedon, V. Bansal, S. K. Bhargava, K. Latham, J. M. Zhu, L. S. Yu, Z. Hu, P. G. Spizzirri, W. Wlodarski and K. Kalantar-zadeh, *Langmuir*, 2009, **25**, 9545.
13. V. Cristino, S. Caramori, R. Argazzi, L. Meda, G. L. Marra and C. A. Bignozzi, *Langmuir*, 2011, **27**, 7276.
14. J. C. Shi, G. J. Hu, R. Cong, H. J. Bu and N. Dai, *New J. Chem.*, 2013, **37**, 1538.
15. M. Figlarz, B. Gerand, B. Dumont and B. Beaudoin, *J. Microsc. Spect. Elec.*, 1980, **5**, A9.
16. A. J. Lindsey and M. Pourbaix, *Chem Ind-London* 1966, **49**, 2038.
17. C. Ng, C. H. Ye, Y. H. Ng and R. Amal, *Cryst. Growth Des.*, 2010, **10**, 3794-3801.
18. J. M. Macak, H. Tsuchiya, A. Ghicov, K. Yasuda, R. Hahn, S. Bauer and P. Schmuki, *Curr. Opin. Solid State M*, 2007, **11**, 3.
19. M. Pourbaix, *Anti-Corros*, 1967, **14**, 28.
20. E. Widenkvist, R. A. Quinlan, B. C. Holloway, H. Grennberg, H and U. Jansson, *Cryst. Growth Des.*, 2008, **8**, 3750.
21. K. Kalantar-zadeh, A. Z. Sadek, H. Zheng, V. Bansal, S. K. Bhargava, W. Wlodarski, J. Zhu, L. Yu and Z. Hu, *Sensors and Actuators B*, 2009, **142**, 230
22. S. B. Zhu, T. G. Xu, H. B. Fu, J. C. Zhao and Y. F. Zhu, *Environ Sci Technol*, 2007, **41**, 6234.
23. M. Radecka, M. Wierzbicka and M. Rekas, *Physica B*, 2004, **351**, 121.

24. Z. L. Jiang, Y. X. Tang, Q. L. Tay, Y. Y. Zhang, O. I. Malyi, D. P. Wang, J. Y. Deng, Y. K. Lai, H. F. Zhou, X. D. Chen, Z. L. Dong, Z. Chen, *Adv Energy Mater*, 2013, **3**, 1368.
25. J. A. Seabold and K. S. Choi, *Chem. Mater.*, 2011, **23**, 1105.

Table of Content

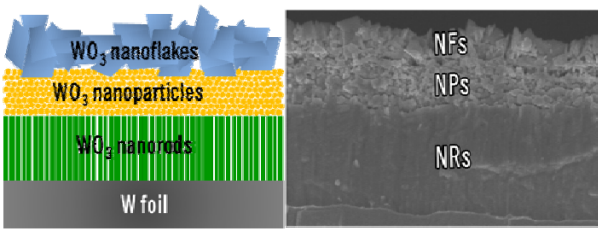

Unique nanorods/nanoparticles/nanoflakes WO_3 triple-layers acting as efficient photoanodes are grown on a metallic W foil by a simple one-step anodization method.